

LIQUID VELOCITY FIELD AND BUBBLE SHAPE MEASUREMENTS IN TWO-PHASE, HORIZONTAL SLUG FLOW

Roberto da Fonseca Junior, robertofonseca@petrobras.com.br
PETROBRAS

Julio Manuel Barros Jr., jmb@puc-rio.br
Departamento de Engenharia Mecânica, PUC-Rio

Luís Fernando A. Azevedo, Lfaa@puc-rio.br
Departamento de Engenharia Mecânica, PUC-Rio

Abstract. *The present paper reports the results of an ongoing project aimed at providing detailed information of the instantaneous liquid velocity field at the film, nose and tail regions of slugs in horizontal two phase flow. To this end, a combination of three non-intrusive optical techniques was employed. Two-dimensional particle image velocimetry (PIV) was used to measure the instantaneous liquid velocity field at a meridional plane of the horizontal pipe test section, while a synchronized pulsed back lighting, provided by a matrix of red LED's, illuminated the bubble contours thereby enhancing contrast of the interfaces (Pulsed Shadow Technique - PST). In order to separate the strong reflections from the gas-liquid interfaces produced by the green PIV laser from the relatively weaker light scattered by the seeding particles required by the PIV technique, a laser-induced fluorescence technique (LIF) was employed. In this technique, tracer particles impregnated with fluorescent dye (Rhodamine B) are used in conjunction with a high-pass optical filter that filters the green light scattered by the interfaces and allow the passage of the fluorescent red light scattered by the tracer particle, thereby allowing for the simultaneous registration of the particle displacement field and bubble shape. The tests were conducted on a specially built transparent pipe test section, using air and water as the working fluids. The velocity fields were obtained for flow regimes where the slugs were lightly aerated, so as to facilitate the utilization of the optical methods described. The velocity field results in the nose, tail and film regions revealed valuable detailed information that contribute to a data bank for supporting the development of two-phase, horizontal slug flow simulations.*

Keywords: *slug flow; PIV; Two-phase flow; Bubble shape; Velocity field*

1. INTRODUCTION

Intermittent two phase flow pattern, which is commonly defined as plug or slug flow, is frequently encountered in industrial applications. Relevant examples are found in oil/gas production and transport lines and in boiler and heat exchanger tubes for energy production plants. Classical flow maps (e.g., Mandhane et al 1974), indicate that the intermittent slug and plug (or elongated bubble) flow regimes exist for a wide range of gas and liquid flow rates in a horizontal two-phase flow configuration.

Due to its intrinsic transient nature, slug flows can cause severe problems in processing and transport equipment due to the intermittent loading that it imposes on the structures. Also in hydrocarbon production lines, where the fluids transported may contain corrosive agents, slug flow is found to present safety risks due to damage imposed on pipe walls. According to Kvernfold et al. (1984), it is believed that the large fluctuations on the wall shear stress imposed by this flow pattern may remove protective corrosion products from the pipe wall facilitating the corrosive-erosive attacks.

The intermittent flow originates from stratified gas-liquid flow when interface waves grow via a classical Kelvin-Helmoltz instability to occupy the entire pipe cross section. At this point, the gas phase propels liquid slugs down the pipe. In front of the moving slug, liquid is collected from the film liquid layer and shed at the slug tail. Observations from several authors (e.g., Sharma and Kosajoy, 1998 and Cook and Behnia, 2000) indicate that short slugs generated at the entry section of a horizontal pipe tend to be only a few pipe diameters long and present a relatively high frequency. As they move downstream along the pipe, short slugs tend to collapse as a result of the trailing gas bubble having higher velocity than the slug front. In this process the frequency of the slugs decreases and stabilizes when most of the slugs are longer than a minimum stable value. The growth of a liquid slug is controlled by the liquid collected from the liquid film under the leading bubble and the liquid shed at the slug tail. For the higher liquid and gas flow rates, gas bubbles entrain the liquid region. For lower flow rates, no bubbles are entrained. Some authors differentiate the two flow regimes calling the former slug flow and the latter, plug flow.

The most significant parameters for the slug flow pattern are the distribution of gas and liquid phases, the liquid velocity and its fluctuating components, the gas bubble frequency (or slug length) and the turbulent transport characteristics of interfacial mass, momentum and energy (Sharma and Kosajoy, 1998). Due to the intermittent and irregular character of the flow, these parameters present time variations. The knowledge of time averaged values of these quantities is not always sufficient for design purposes, and statistical information might be relevant. For instance, the design of slug catchers has to be based on the longest possible slug, and not on the average one.

Physical modeling of horizontal slug flow has been the focus of several studies in the literature. Traditional models are normally based on the unit-cell approach for fully developed slugs, where mass and momentum equations are

applied to a control volume around a long gas bubble and the liquid slug, using a frame of reference moving along with the cell (Wallis, 1969, Dukler and Hubbard, 1975 and Taitel and Barnea, 1990). A different approach for modeling slug flow is obtained with the statistical cell model, which is able to predict some intermittency characteristics by conditional averaging of the conservation equations (e.g. Fabre and Liné, 1992). Slug tracking are transient flow models that attempt to predict the motion, growth and disappearance of slug by tracking individual slugs. The position of each slug tail and front in time is monitored along the pipe using Lagrangian coordinates. This information is used in mass and momentum balances at the slug front and tail. Empirical correlations are needed to close the model (e.g., Bendiksen et al., 1990, Barnea and Taitel, 1993). Issa et al., 2003, describes a slug capture technique based on a two-fluid, one dimensional transient model in which the slug flow regime is predicted by a mechanistic model where the slug occurs as a consequence of the growth of hydrodynamic instabilities obtained by the solution of the transport equations for mass and momentum for each phase. Empirical information is minimized in this model, being only necessary for liquid-wall, gas-wall and interfacial shear forces

As the brief review of modeling efforts presented above reveals, detailed experimental information on the relevant flow properties are necessary to improve the modeling capabilities. Besides, due to complexity of the slug flow pattern, experimental information is of fundamental importance to provide new insights on the physical mechanisms involved in the flow.

The objective of the present paper is to present the results of an ongoing research effort aimed at the development and application of non-intrusive, optical-based techniques for the determination of local, instantaneous information on the flow field and bubble shape in the plug and slug flow regimes. As will be described shortly, the techniques implemented, although not original, provide detailed information of the instantaneous flow field over extended regions in the liquid slug and within the film layer around the bubble nose and tail. The technique also yields useful information on the instantaneous bubble interface shape. Before presenting the details of the technique implemented, a brief overview of the literature on experimental studies conducted on slug flows will be presented.

2. LITERATURE REVIEW

A literature search reveals a large number of papers presenting experimental investigations of the global characteristics of slug flows. These experiments were conducted to support the development and verification of slug flow models in the horizontal configuration. In these studies, the focus is on global measurements such as pressure drop, overall void fraction and statistical parameters such as slug length distribution, slug frequency and film thickness (e.g., Bendiksen, 1984, Cook and Behnia, 2000, Bertola, 2002, Hout et al., 2003, Xin et al., 2006). Probably due to the complex nature of the slug flow pattern, relatively few papers were found reporting results on detailed measurements of the flow field in the liquid slug and film layer under the gas bubble. Detailed information on the flow behavior is critical to the proper understanding of the physical mechanisms governing the flow.

Kvernøld et al (1984) conducted a study in which velocity profiles were measured in the film and liquid slug regions. A LDV (Laser Doppler Velocimetry) probe was employed together with a specially designed data validation algorithm to account for the unwanted light scattered by the bubbles present in the liquid. The technique presented successful results only in situations where there was a small bubble concentration entrained in the liquid. The velocity profiles reported were in good agreement with the accepted slug dynamics derived from macroscopic data.

Shemer & Barnea (1987) developed a method to characterize the instantaneous velocity profiles of liquid slug in vertical and horizontal flow using the hydrogen bubble technique. They observed variations of the local maximum and fluctuating liquid velocity associated with the motion of the gas bubble away from the wall. It was also concluded that the liquid instantaneous velocity profile directly influences the shape of the bubble nose. Kawaji (1998) also studied the liquid velocity profiles using the non-intrusive technique known as PDA (Photochromic Dye Activation), whereby dye dissolved in the liquid is activated externally. The author presented instantaneous velocity profiles near the gas-liquid interface.

Sharma et al (1998) and Lewis et al (2002) employed the hot film technique to obtain the most detailed local velocity data available to that date on slug flows. They employed two hot film probes simultaneously; one was kept fixed and provided the phase data, while the second probe was traversed to measure the liquid velocity. Time-averaged local void fraction distribution, velocity profiles and turbulent data were presented for the liquid slug and liquid film. Strong shear layers were identified at the top of the film layer. The relative importance of the bubble-induced turbulence was identified. Regions presenting lower turbulence levels than the single phase flow were identified close to the lower wall in the slug region and were linked to the *lubricating* effect caused by the small bubbles flowing close to the bottom part of pipe wall.

Gomez (2003) presented a detailed experimental study of the velocity distribution in both the slug and the liquid film, using the LDV technique. In the experiments the gas bubble was held stationary by a counter flow imposed in the inclined tube. The presence of small bubbles entrained in the liquid induced noise in the Doppler signal. The higher energy signals scattered from the bubbles were filtered to allow the measurement of the seed particle's signal. The low signal sampling rate obtained precluded the measurement of turbulent spectra. Time averaged and standard deviations of the axial and radial velocity components were obtained. Time-averaged axial velocity profiles in the slug upstream of

the bubble were well correlated by $1/7^{\text{th}}$ power law profile. Three flow regions were identified in the slug according to the velocity profiles obtained: separated, transition and fully developed region.

Instantaneous full field measurements of the liquid phase in slug flow were reported by Carpintero-Rogero et al, 2006. The author employed three simultaneous optical techniques to produce time-averaged and turbulent data for the liquid slug and film layer. Since the techniques employed in that paper were the same as those of the present paper, the description of the techniques will be presented in the next section.

As indicated in this brief summary of the main efforts directed toward the determination of detailed information on the velocity field in liquid slugs, the transient nature of the slug flow regime poses a limitation on the use of point-measuring techniques, such as LDV and hot film. The possibilities open by the new full field techniques such as PIV, now largely employed in single phase measurements, might contribute to a better understanding of the physical phenomena of this complex flow. However, as will be commented in the next section, optical access and the random gas-liquid interfaces are sources of limitations to these techniques.

3. MEASUREMENT TECHNIQUE

This section presents a brief description of the optical techniques employed in the studies reported in the present paper. The main technique used to measure the instantaneous velocity field in the liquid slug was the Particle Image Velocimetry – PIV. Due to the presence of the gas-liquid interfaces characteristic of the intermittent flow, other two optical techniques were applied simultaneously. A description of these techniques is presented next.

3.1. Particle Image Velocimetry (PIV)

The particle image velocimetry technique (PIV) has been widely used in the last decade to perform measurements of the instantaneous velocity fields in single phase flows. Its basic principle can be explained with the aid of Fig. 1(a), obtained from DANTEC Dynamics. A double pulse of a laser light sheet illuminates the flow area of interest. The consecutive light pulses are closely spaced in time (typically, a few micro seconds interval between pulses). Two images of small seeding particles previously distributed in the flow are recorded by a digital camera and stored in a computer. The images are subdivided into small areas denominated interrogation windows. The sizes of these windows determine the spatial resolution of the technique. Typical resolutions are of the order of half a millimeter or smaller. The velocity field is determined from the displacement field of the tracer particles and the knowledge of the time interval between pulses. A cross-correlation procedure is used to determine the average particle displacement within each interrogation window. In a standard PIV application thousands of instantaneous velocity vectors are measured in the illuminated area. The accuracy of the velocity measurement is of the same order as that for the point techniques such as LDV and hot wire anemometry (typically of the order of 1%).

It is common that a small number of spurious vectors are obtained from the cross correlation procedure. Possible reasons for those bad vectors are the lack of sufficient particles in the interrogation window, excessive velocity gradients, out of plane motions, wall reflection, etc. Those vectors are normally eliminated by a post processing procedure and, if desired, substituted by interpolated vectors. A complete description of the PIV technique can be found in the book by Raffel et al., 2007.

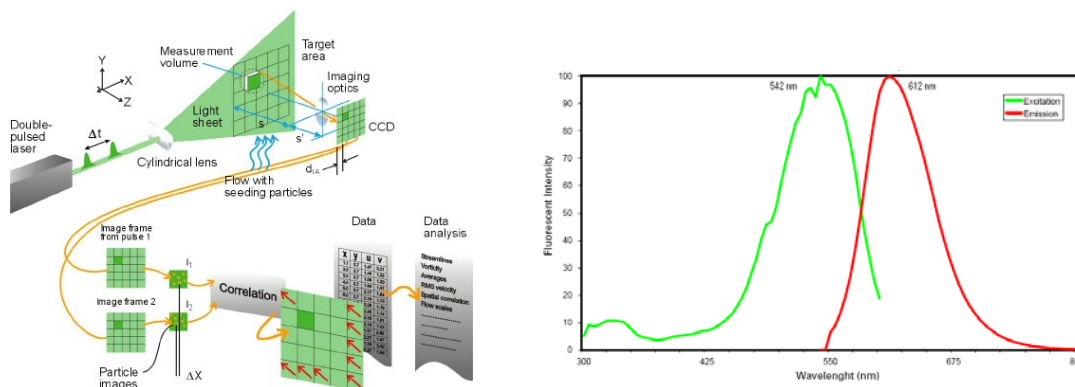


Figure 1- (a) Principle of operation of the PIV technique. (Source: www.dantecdynamics.com). (b) Spectrum of absorption and fluorescence material (Source: Thermo Scientific).

3.2. Laser Induced Fluorescence (LIF)

In order to allow the application of the PIV technique to two-phase flows, it is necessary to devise a method to avoid that the intense reflections from the laser light sheet on the liquid-gas interfaces blocks the capture of the relatively much less intense light scattered by the small tracer particles. This can be accomplished by the use of the Laser Induced Fluorescence (LIF) technique. This is an optical technique based on the property of some organic molecules that once excited at certain wavelength emit light at a different wavelength. Figure 1(b) presents a typical absorption and fluorescence spectrum of a fluorescent material. In the figure the abscissa represents the wavelength of light and the ordinate the intensity of the light. The green curve represents the absorption curve of a substance, showing a peak at the wave length 542 nm, which corresponds to the green light normally found in the lasers used for PIV applications. The red curve represents the fluorescence emission, which, for this particular substance, peaks at 612 nm, corresponding to red light.

The liquid phase of the two-phase flow is seeded with fluorescent particles and illuminated with the green laser sheet. If a high pass optical filter with cutoff wavelength at, say, 520 nm is placed in front of the digital camera, only the red light from the fluorescent particles will be registered by the camera and the green light from the interfaces will be filtered out.

3.3. Pulsed Shadow Technique (PST)

The Pulsed Shadow Technique (PST) (Lindken and Merzkirch, 2002) is used in conjunction with the PIV and LIF techniques to improve the definition of the bubble contours in two-phase flow measurements. The technique consists in employing a uniform background illumination to improve the contrast of the gas phase during a PIV image recording. Without the use of this background illumination, the contours of gas bubbles present in the flow appear in the recorded digital image as a region free of seed particles. The boundary between seeded and non seeded flow is taken as the bubble contour. This procedure, however, does not provide a sharp definition for the interfaces. The use of background lighting synchronized with the camera capture improves the interface contrast. In order for this technique to be used with the LIF technique, it is necessary that the wavelength of the background illumination be compatible with the high-pass optical filter used to block the green laser light. In the present experiments a panel formed by 132 high-power, low-emission-angle, LEDs emitting at 640 nm was employed.

4. EXPERIMENTAL FACILITY

Figure 2 schematically presents the test section constructed to conduct the experiments. A 24-mm-diameter, 10-meters-long Plexiglas pipe was mounted on a rigid steel frame that could be rotated around a pivot to produce inclination angles between 0 and +10° with the horizontal. In the present paper only results for the horizontal cases will be presented. The pipe length-to-diameter ratio was 400, which should be sufficient for the formation of stable slugs. Water from a reservoir was pumped in closed circuit through the test pipe by a progressive cavity pump. A centrifugal blower provided compressed air for the test section. Calibrated rotameters were used to measure the water and air flow rates. Air and water were mixed at a Y-junction positioned at the entrance of the Plexiglas pipe. After passing through the test pipe, the two-phase mixture returned to the reservoir where a tangential inlet aided the phase separation process. The green and blue arrows in Fig. 2(a) indicate, respectively, the water and air flow paths in the test section.

The measuring section was located at 350 diameters from the pipe entrance. As can be seen schematically in Fig. 2(b), the measuring section was specially prepared to receive the components necessary for the implementation of the three optical techniques employed in the experiments, namely, PIV, LIF and PST. Light from a double cavity, 120-mJ, Nd-YAG laser manufactured by New Wave was shaped into a plane sheet and directed to the meridional vertical plane of the pipe. A set of cylindrical and spherical lenses was used to form the light sheet that presented approximate dimensions in the measuring region of 50 x 0,5 mm (width x thickness). A 45° mirror was also employed to divert the laser beam that entered the test section from below, as indicated in the figure. In order to minimize reflections from the laser light at the curved pipe surface, a rectangular glass box was mounted around the pipe at the measuring area. The box was filled with water.

The maximum firing frequency of each laser cavity was 15 Hz. The dual cavity laser system allows for very short pulse intervals between laser firing. Typical pulse intervals of the order of micro seconds can be easily achieved, which is adequate for measuring liquid velocities significantly higher than the levels encountered in the experiments conducted. The laser was operated to emit green light at a wavelength of 532 nm. The particle images were acquired by a PIVCAM 10-30 digital camera manufactured by TSI. The camera can be operated in the frame straddling mode, which allows for the capture of pairs of consecutive images with time intervals in the micro second range. Pairs of consecutive images can be acquired by the camera at 15 Hz, which is compatible with the laser firing frequency. The camera offered a 1000 x 1000 pixel resolution. As indicated in the figure, the camera was mounted orthogonally to the

light sheet plane. A 50-mm focal distance lens was used in the experiments. The panel of LED's for the background illumination required by the PST technique was mounted on the opposite side of the camera. A sand-blasted diffuser glass plate was positioned in front of the LED panel to improve the spatial uniformity of the background illumination. The high-pass optical filter required for the LIF technique was fixed on the rectangular glass box in the viewing path of the camera. In the present study seeding was obtained with the use of 15- μm -diameter fluorescent particles with peak excitation wavelength at 542 nm and peak fluorescence emission at 612 nm. The particles density was 1.05 g/cm^3 .

A photogate cell was installed around the pipe, upstream of the glass box. This cell (not shown in the figure) provided trigger signals for the velocity measuring system. The cell output a high voltage signal when gas passes through the cell, and a low voltage signal when water is flowing through. The transition from a high to low voltage signal is an indication of the passage of a gas-liquid interface at the photogate position. A controlling circuit triggered by the photogate signal outputs a trigger signal to the velocity measuring system after a pre-set time delay. By controlling the time delay, it was possible to always measure the liquid velocity field at a pre-determined position in relation to the gas bubble surface position. A second photogate cell was installed at a known position from the first one and was employed in the measurement of statistical slug properties, such as length, frequency and velocity distributions. No slug statistical results will be presented in the present paper.

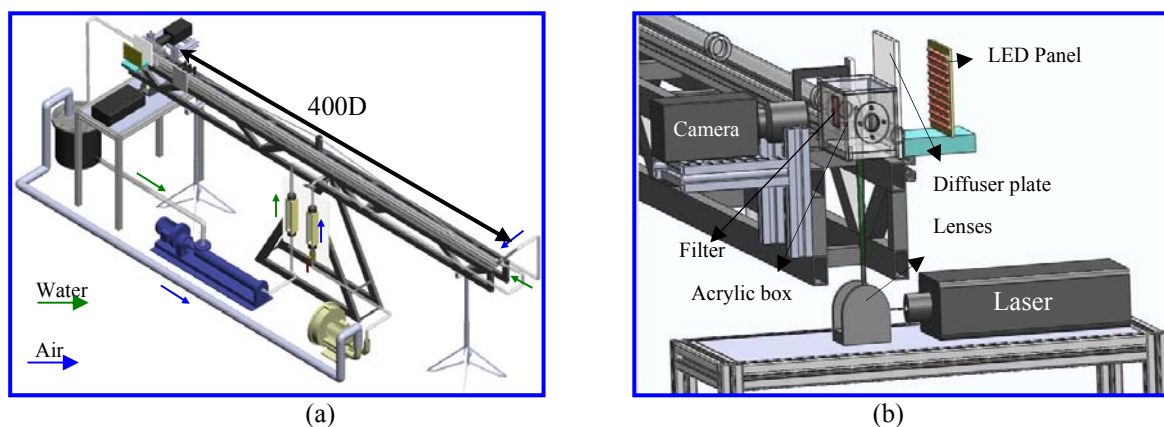


Figure 2 – (a) Overview of test section. (b) Components of the velocity and bubble shape measuring system.

5. EXPERIMENTAL PROCEDURE AND IMAGE PROCESSING

The measurement procedure utilized in the determination of the instantaneous velocity field around a bubble and the bubble contour will now be described. A data run was initiated by setting the desired air and water flow rates. A computer controlled synchronizing circuit was responsible for activating the components of the measuring system with precise timing. When a gas-liquid interface reached the photogate cell, a trigger signal was sent to the synchronizer circuit that, after a pre-set delay, activated the LED matrix, fired the two laser pulses with the pre-defined time interval and triggered the camera for the capture and storage of the pair of images that would later be processed to yield the desired vector field. Different time delays were set depending on whether the flow field to be measured was at the neighborhood of the bubble nose or tail. The time interval between laser pulses was determined as a function of the maximum displacement allowed for the tracers particles that yield good image correlation. This routine was repeated for subsequent bubble trigger signals at a rate of 15 Hz.

An image acquired by the simultaneous use of the PIV, LIF and PST techniques display three distinct levels of pixel intensities, or in terms of black and white images, distinct gray levels. The fluorescent particle images display the highest gray levels, followed by background of the liquid region around the bubble. The gray levels within the region limited by the bubble are the lowest in the image.

A special image processing procedure was devised to prepare the images to be processed by the PIV cross correlation algorithm. Firstly, a reference image was acquired of the stagnant liquid in the pipe, without any gas bubbles present. A median filter (Nogueira et al. 2003) was applied to the image with the objective of removing the particles signal that shows in the image as a high spatial frequency. Next, the same filter was applied to the original image of the flow with the bubble contour present. Figure 3(a) shows an example of such an image, before the median filter was applied. The bubble contour and particle images can be seen in the figure. The filtered reference image was then subtracted from the filtered original image. This operation produces a uniform background and enhances the bubble contour. Next, this image was binarized using an adequate threshold value, resulting in a sharp bubble contour that would be later used as a mask. Figure 3(b) displays the binarized mask obtained. In the final stage of the image processing procedure, the original image was multiplied by mask resulting in an image with only the liquid region with

the particles and a blackened bubble region, as seen in Fig. 3(c). A pair of these processed images corresponding to the two laser pulses was input to the cross correlation algorithm that calculated the velocity field.

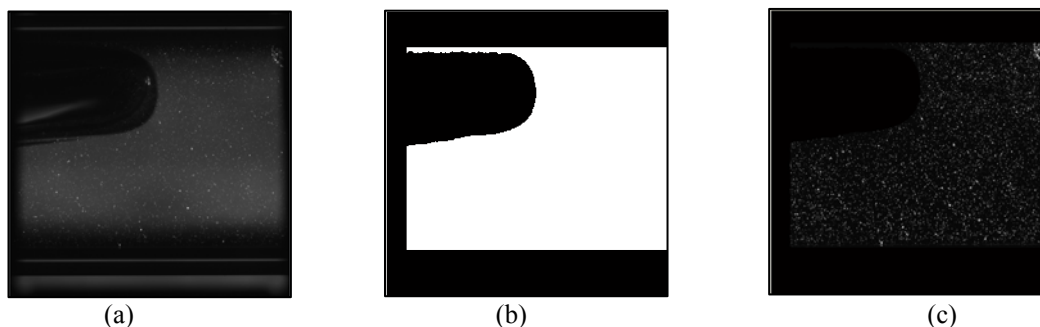


Figure 3 – Image processing procedure: (a) Original Image; (b) Binarized mask (c) Final PIV image.

For the determination of the particle displacements the Insight software developed by TSI was employed. This software uses an adaptive correlation based on a Fast Fourier procedure, using rectangular correlation windows. A Gaussian-peak fit was employed to determine the correlation peak with sub-pixel accuracy. A typical window size utilized was 32 x 16 pixels, which corresponded to a 1 x 0.5 mm window size in the actual flow .

6. RESULTS

The results obtained with the techniques described will now be presented. The aim of this presentation is not to explore the physics of intermittent two phase flow, but, rather, to display the potential of this measuring technique as a research tool.

Table 1 displays the test matrix investigated in the studies conducted. A plot of these liquid and gas flow rate pairs in a flow pattern map such as that proposed by Mandhane et al (1974) shows that the tests covered a region of elongated bubbles (plug flow) up to the transition to slug flow.

Table 1 – Test Matrix Investigated

Test	U _{ls} (m/s)	U _{gs} (m/s)	U _{mist} (m/s)	Froude	<Lb>	<Lp>
1	0.3	0.5	0.8	1.6	77D	18D
2	0.4	0.5	0.9	1.8	52D	15D
3	0.5	0.5	1	2.1	29D	13D
4	0.3	0.8	1.1	2.3	115D	19D
5	0.4	0.8	1.2	2.5	77D	16D
6	0.5	0.8	1.3	2.7	60D	16D

The test matrix presents the superficial liquid velocity, U_{ls}, the superficial gas velocity, U_{gs}, and the mixture velocity U_{mist}, which represents the sum of the phase velocities. Also presented in the table is the Froude number defined by equation 1. In this equation, ρ_L is the density of the liquid, Δρ is the difference between the liquid and gas densities, D the internal pipe diameter and g the acceleration of gravity. For reference purposes, the last two columns of Table 1 present the average, dimensionless bubble and slug lengths measured by the photogate cells described previously.

$$Fr = U_{mist} / [(\Delta\rho / \rho_L) g D]^{1/2} \quad \text{Eq. 1}$$

The image processing procedure described in the previous section yielded, in one its intermediate steps, the binarized bubble contour shape. Since the bubble contour was available in each recorded image, the evolution of the bubble shape was also available for analysis. The use of a high frame rate camera in conjunction with the techniques described would provide time resolved bubble shape evolution. As an example, Figure 4 presents bubble contours recorded for the conditions of tests 1 and 6. These tests represent, respectively, the minimum and maximum mixture velocities investigated. These images confirm the findings reported in the literature (Bendiksen, 1984) that indicates that the bubble tip tends to move toward the pipe centerline as the mixture velocity increases. This behavior is believed to be a consequence of the flow separation at the leading bubble tail that displaces the maximum fluid velocity in the liquid slug toward the top of the pipe, downstream of the separated region. The momentum flux displaced to the upper part of the pipe produces a force on the trailing bubble that tends to move its nose toward the pipe centerline, as confirmed by the pictures of Fig. 4.

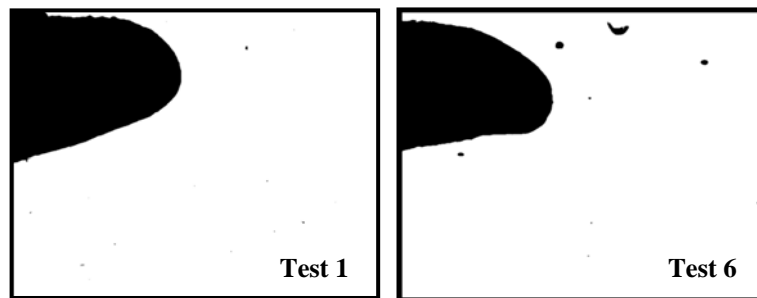


Figure 4 – Bubble shape for small and large mixture velocities.

6.1. Instantaneous velocity field

Figures 5 and 6 display the representative results obtained for the instantaneous two-dimensional velocity field obtained by the techniques implemented. Figure 5 presents the instantaneous velocity fields in a region around the bubble nose for the minimum and maximum mixture flow rates characterized by the parameters of test cases 1 and 6. For the same test cases, Figure 6 presents the instantaneous velocity field at the bubble tail. It is worth noting the high spatial resolution obtained for the velocity measurements. The velocity vectors are color-coded by velocity magnitude, the red color representing the higher velocity levels.

A comparison of the two flow maps of Fig 5 reveals the tendency of the flow ahead of the bubble nose assuming a flat shape in most of the pipe cross section, as the mixture velocity is increased. As seen in Fig. 6, the instantaneous measuring technique employed captured some interesting flow characteristics in the bubble tail region. A strong, jet-like flow was captured at the exit plane of the film layer under the bubble, where a marked shear layer is formed. This jet-like flow has been reported by the hot-film measurements of Lewis et al., 2002, although, due to the limitations of the point-measuring technique employed in that paper, information was presented for only one axial velocity position. The higher mixture velocity of test case 6 presented in Fig 6(a) already show the presence of detached gas bubbles in the liquid slug region in the form of areas free of vectors.

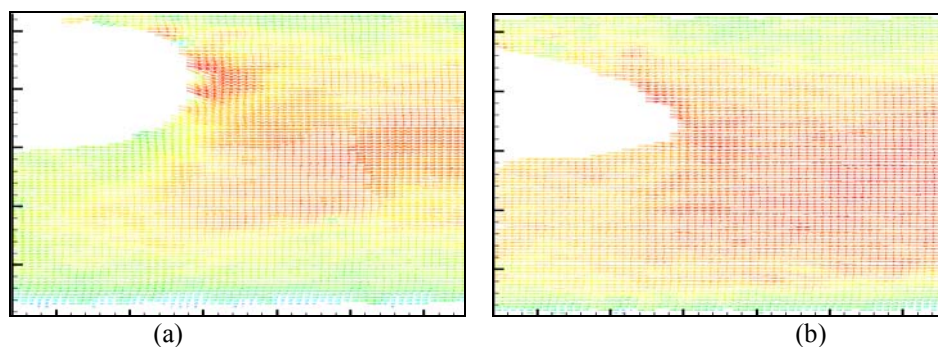


Figure 10 – Instantaneous velocity field at the bubble nose region. (a) Test 1 - (b) Test 6.

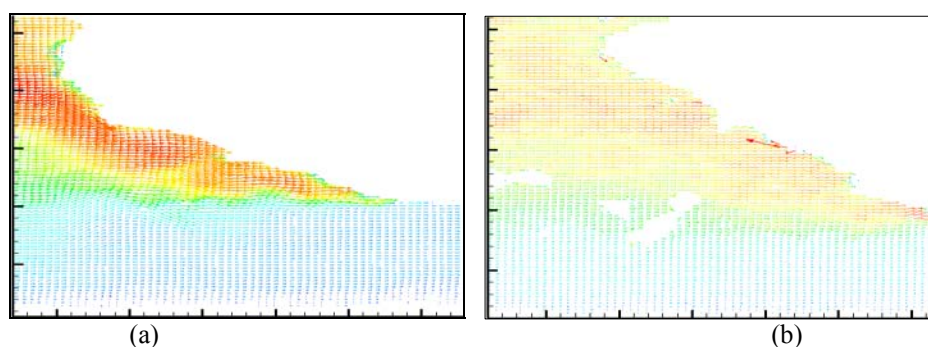


Figure 6 – Instantaneous velocity field at the bubble tail region. (a) Test 1 - (b) Test 6.

New insights into the instantaneous flow field can be obtained if the velocity vectors are displayed in relation to a frame of reference that moves along with the bubble nose velocity, as presented in Figures 7 and 8, respectively for test cases 1 and 6. In Fig. 7 one can observe that, for both test case conditions, the bubble moves faster than the liquid slug, as indicated by the liquid flow directed to the left. Also, Fig. 7(b) shows clearly the downward flow acting at the bubble

nose responsible for its motion toward the pipe centerline, as commented before. At bubble tail, Fig. 8, the change of reference allows for a clear visualization of the recirculation zone formed as the jet-like flow expands to fill the large slug area.

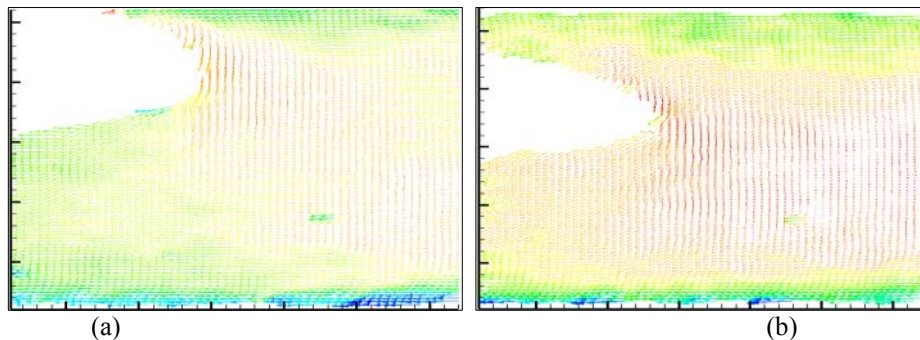


Figure 6 – Flow field at the bubble nose region for the moving frame of reference. (a) Test case 1 (b) Test case 6.

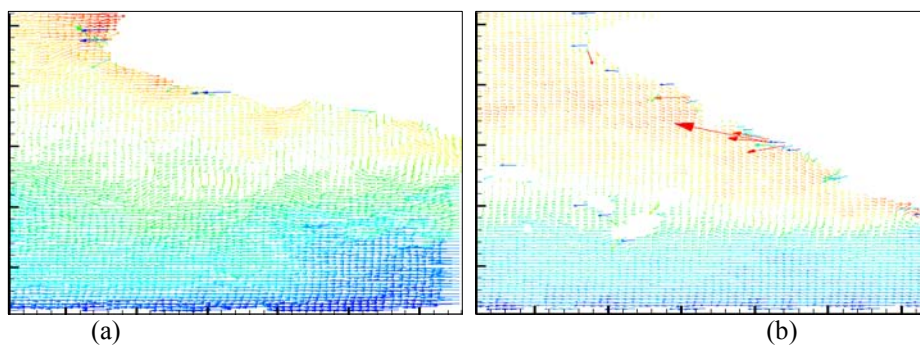


Figure 7 – Flow field at the bubble tail region for the moving frame of reference. (a) Test case 1 (b) Test case 6.

6.2. Average velocity profiles

Average velocity profiles in the axial (u) and radial (v) directions were obtained from instantaneous flow fields such as those just presented. The intermittent character of the bubbles produces images of bubbles of different shapes in each instantaneous velocity field measured. Thus, the axial location for each profile has to be referenced to a determined position of the bubble contour in order to allow the ensemble averaging of profiles extracted from different instantaneous flow fields. In our study, reference was made to the tip of the bubble nose. Due to space limitations and not to overcrowd the presentation, only selected average profiles of axial velocity are presented in Fig. 8 and 9. Besides the profile at the bubble tip location, velocity profiles are presented in Fig. 8 for axial positions of 0.2, 0.4, 0.6 and 0.8 pipe diameters downstream of the bubble. Those are the profiles in the slug region in front of the gas bubble. The profiles in the film region under the bubble are presented in Fig. 9 for the axial positions -0.2, -0.4, -0.6 pipe diameters upstream of the bubble nose tip. Each figure presents results for test cases 1 and 6. All the profiles presented were obtained from ensemble averaging over $N=150$ instantaneous profiles, according to equation 2,

$$\bar{u}(x, y) = \frac{1}{N} \sum_{i=1}^N u_i(x, y) \quad \bar{v}(x, y) = \frac{1}{N} \sum_{i=1}^N v_i(x, y) \quad (\text{Eq. 2})$$

A general observation of Fig. 8 shows that the axial velocity profiles attain a fully developed condition at very short distances from the bubble nose, for both mixture flow velocities corresponding to test cases 1 and 6. Indeed, with the exception of the profile at the nose location, all other profiles are nearly coincident. In fact, comparisons made with the $1/7^{\text{th}}$ power law profile corroborate this observation. At the nose location the profiles present a s-shape, reflecting the influence of the bubble velocity. Also worth noting, is the influence of the bubble velocity on the axial profiles at all axial locations. A comparison of the results for test cases 1 and 6 show a downward motion of the maximum velocity position that follows the downward motion of the bubble nose tip.

The axial velocity profiles for the three axial positions located in the film layer shown in Fig. 9 reveal an acceleration of the flow in the film toward the nose region, for both test case conditions. The higher mixture velocities that characterize test 6 can be noted in the profiles. Since the film thickness is approximately the same in the two cases, higher shear stress levels at the pipe wall prevail for case 6.

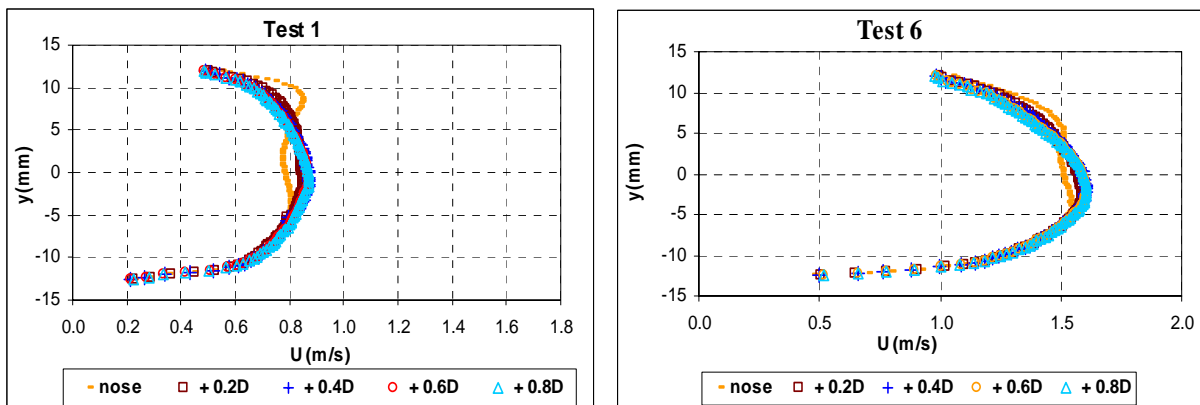


Figure 8 –Profiles of axial velocity downstream of the bubble nose.

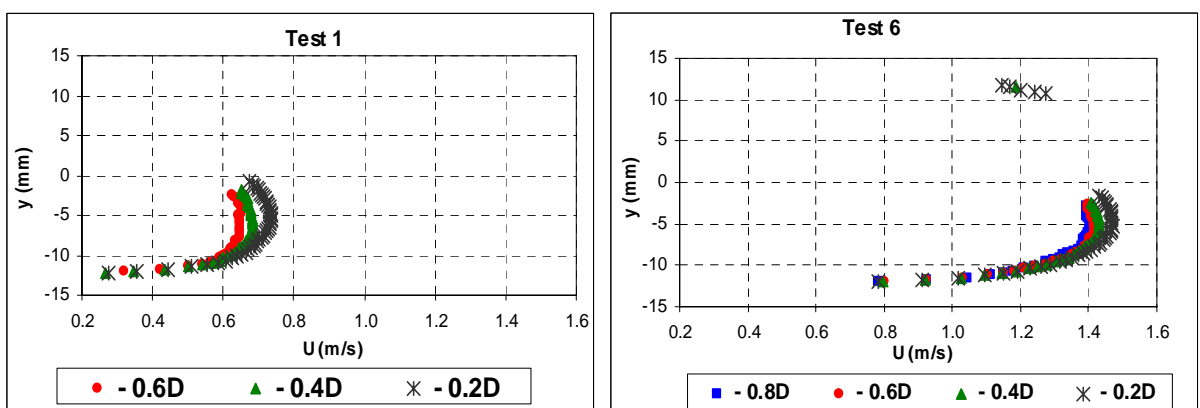


Figure 9 –Profiles of axial velocity in the film region

7. CONCLUSION

The present paper described an ongoing research project aimed at developing non intrusive, optical techniques for measuring instantaneous velocity fields for two-phase flow. In the present case, attention was focused on the horizontal plug flow of water and air. Strong reflections produced by the illuminating laser light at the gas-liquid interface preclude the use of the Particle Image Velocimetry technique in its standard form normally used for single flow measurements. Two additional optical techniques were employed to overcome this limitation. Laser Induced Fluorescence and Pulsed Shadow techniques were employed in conjunction with PIV. High pass optical filters were used to filter the green light reflected by the interfaces and allow the passage of the red light from fluorescent particles distributed in the flow. A panel of LED's furnished back light illumination to enhance the bubble contours.

Instantaneous velocity fields were obtained for the region downstream of the bubble nose and at the bubble tail for plug flow regime. Detailed information was obtained from the high spatial resolution vector field.

Averaged velocity profiles were obtained at selected location in the nose and film regions.

The results obtained demonstrated that the combinations of the three optical techniques form a powerful research tool to explore two phase flows. Further development needs to be performed to overcome the current limitations of conducting measurements in highly aerated slug flows.

8. REFERENCES

- Barnea and Taitel, 1993, A model for slug length distribution in gas-liquid slug flow, *Int. Journal of Multiphase Flow*, Vol. 19, pp. 829-838.
- Bendiksen, K., 1984. An experimental investigation of the motion of long bubbles in inclined tubes. *Int. Journal of Multiphase Flow* Vol. 10, pp. 467-483.
- Bendiksen, K., Saeter, G., Muller J., Froland E., 1990. The fractal statistics of liquid slug. *Int. Journal of Multiphase Flow* Vol. 16, pp. 1117-1126.

- Bertola, V., 2002, Slug velocity profiles in horizontal gas-liquid flow, *Experiments in Fluids*, Vol. 32, pp. 722-727.
- Carpintero-Rogero, E., Kroess, B., Sattelmayer, T., 2006, Simultaneous HS-PIV and shadowgraph measurements of gas-liquid flows in a horizontal pipe. 13th Int. Symp. on Applications of Laser Techniques to Fluid Mechanics.
- Cook, M. and Behnia, M., 2000, Slug length prediction in near horizontal gas-liquid intermittent flow. *Chemical Engineering Science*, Vol. 55, pp. 2009-2018.
- Dukler, A. E., Hubbard, M.G., 1975, A model for gasliquid slug flow in horizontal and near horizontal tubes. *Industrial and Engineering Chemistry Fundamentals*, Vol. 14, Nr. 4, pp. 337-347.
- Fabre, J., Liné, A., 1992, Modelling of two phase slug flow. *Annual Reviews Fluid Mech.*, Vol. 24, pp. 21-46.
- Gomez, A.H., 2003, Interaction hydrodynamique entre deux poches de gaz en tube, Institut National Polytechnique of Toulouse, Dissertation.
- van Hout, R., Shemer, L., Barnea, D., 2003, Evolution of hydrodynamic and statistical parameters of gas-liquid slug flow along inclined pipes, *Chemical Engineering Science*, Vol. 58, pp. 115-133.
- ISSA, R.I. ; KEMPF, M.H.W., 2003, Simulation of slug flow in horizontal and nearly horizontal pipes with the two-fluid model. In: *International Journal of Multiphase Flow*, Vol. 29, pp. 69-95.
- Kawaji, M. , Ali, M.I., Ciastek, A., Lorencez, C.M., 1995. Study of liquid flow structure in horizontal cocurrent gas-liquid slug flow. *ANS Proc. 30th ASME/AIChE/ANS/AIAA National Heat Transfer Conference*, 5-9 August, Portland, Oregon, pp. 79-88.
- Kvernfold, O., Vindoy, V., Sontvedt, T., Saasen A. and Selmer-Olsen S., 1984, Velocity distribution in horizontal slug flow. *International Journal of Multiphase flow*, vol.10, n°. 4, pp. 441-457.
- Lewis, S., Fu, W.L., Kojasoy, G., Internal flow structure description of slug flow-pattern in a horizontal pipe *Int. Journal of Heat and Mass Transfer*, vol. 45, pp. 3897-3910.
- Lindken, R. and , Merzkirch, W., 2002, A novel PIV technique for measurements of multiphase flows and its application to two phase bubbly flow, *Experiments in Fluids*, 33:814-825.
- Mandhane, J.M., Gregory, G.A. and Aziz, K.. Flow-pattern map for gas-liquid flow in horizontal pipes, *International Journal of Multiphase Flow*, 1, 1974, p-537.
- Nogueira, S. ; Sousa, R. G. ; Pinto, A. M. F. R. ; Riethmuller, M. L. ; Campos, J. B. L. M., 2003, Simultaneous PIV and pulsed shadow technique in slug flow: a solution for optical problems. *Experiments in Fluids*, vol. 35, pp. 598-609.
- Raffel, M., Willert, C., Wereley, S., Kompenhans, J., 2007, *Particle Image Velocimetry – A Pratical Guide*. Second Edition, ed. Springer. ISBN 978-3-540-72307-0.
- Sharma, S. Lewis, S. Kojasoy G. Local studies in horizontal gas-liquid slug flow. **Nuclear Engineering and Design**, 184, 1998, p. 305-318.
- Shemer, L., & Barnea, D., 1987, Visualization of the instantaneous velocity profiles in gas-liquid slug flow. *Physicochemical Hydrodynamics*, Vol. 8, n.3, pp.243-253.
- Taitel, Y., Barnea, D., 1990, Two-phase slug flow. *Advances in Heat Transfer*, Vol. 20, pp. 83-90.
- Wallis, G. B., 1969, *One dimensional two-phase flow*. New York: Mc Graw-Hill.
- Wang, X., Guo L. and Zhang X., 2006, Development of liquid slug length in gas-liquid slug flow along horizontal pipeline: Experiment and simulation, *Chinese J. Chem. Eng.*, vol. 14, pp. 626-633

9. ACKNOWLEDGMENT

The authors gratefully acknowledge the support awarded to this research by PETROBRAS and CNPq – Brazilian Research Council.

10. RESPONSIBILITY NOTICE

The authors are the only responsible for the printed material included in this paper.